LETTERS
https://doi.org/10.1038/s41566-019-0492-5

nature photonics

Graphene photonic crystal fibre with strong and tunable light–matter interaction

Ke Chen[1,2,7], Xu Zhou[3,7], Xu Cheng[3,7], Ruixi Qiao[3], Yi Cheng[1,4], Can Liu[3], Yadian Xie[1,4], Wentao Yu[3], Fengrui Yao[3], Zhipei Sun[5], Feng Wang[6], Kaihui Liu[3*] and Zhongfan Liu[1,4*]

The integration of photonic crystal fibre (PCF) with various functional materials has greatly expanded the application regimes of optical fibre[1–12]. The emergence of graphene (Gr) has stimulated new opportunities when combined with PCF, allowing for electrical tunability, a broadband optical response and all-fibre integration ability[13–18]. However, previous demonstrations have typically been limited to micrometre-sized samples, far behind the requirements of real applications at the metre-scale level. Here, we demonstrate a new hybrid material, Gr–PCF, with length up to half a metre, produced using a chemical vapour deposition method. The Gr–PCF shows a strong light–matter interaction with ~8 dB cm^{-1} attenuation. In addition, the Gr–PCF-based electro-optic modulator demonstrates a broadband response (1,150–1,600 nm) and large modulation depth (~20 dB cm^{-1} at 1,550 nm) under a low gate voltage of ~2 V. Our results could enable industrial-level graphene applications based on this Gr–PCF and suggest an attractive platform for two-dimensional material-PCF.

Graphene is a promising material in photonic and optoelectronic applications due to its superior properties of high carrier mobility, broadband optical response and facile electrical tunability, which originate from its unique linear dispersion of massless Dirac fermions[19–28]. Although the light–matter interaction in graphene, normalized by its atomic thickness (0.34 nm), is quite strong, the measurable interaction is in fact quite weak (only ~2.3% light absorption)[29]. To enhance the light–graphene interaction, many efforts have been devoted to combining graphene flakes with well-designed optical structures, such as gratings, waveguides and microcavities[30–34]; however, all these hybrid structures have had a sample size on the scale of micrometres, rather than metres, which limits their widespread applications. There is thus a great demand to develop new methods for the mass production of graphene-based optical structures for material-level applications.

Optical fibre provides the highest-quality optical waveguide for information communication and photon manipulation, and it has been mass manufactured at a length scale of kilometres. The development of photonic crystal fibre (PCF) is the most important advance in optical fibre in the last 20 years, with its extremely rich functions beyond traditional optical fibre in the exciting applications of endlessly single-mode fibres, supercontinuum lasers, frequency combs, optical soliton propagation, high-power pulse delivery and so on[1–7]. PCF, with its ingenious porous structure, has opened up opportunities based on filling it with a range of materials, from gases, liquids and solids to liquid crystals, thus expanding its functionality to mode-locked fibre lasers, laser frequency conversion, surface plasmon generation, stimulated Raman scattering and in-fibre thermal- or electro-optic devices[8–15]. The emergence of two-dimensional (2D) graphene has now stimulated keen interest in combining PCF with graphene. A graphene–PCF (Gr–PCF) complex provides several unique advantages: (1) the flexibility of graphene facilitates its tight attachment to the hole walls of the PCF; (2) the atomic thickness of graphene keeps the PCF structure and main optical functions intact and (3) the distinct properties of graphene bring unique functions that cannot be realized by any other conventional material. Indeed, great efforts have been made to fabricate a graphene–optical fibre complex by transferring graphene flakes onto side-polished or tapered normal optical fibres[16–18], or filling them into the holes of PCFs[13–15]. However, all these attempts have only been accomplished on the scale of micrometres and with a small interaction area and harmful effects on the fibre modes, and an efficient and non-harmful manufacturing strategy for the mass production at a metre scale of Gr–PCF complexes (with large interaction area and intact structure) has yet to be found.

In this Letter, we report the production of a new hybrid material, Gr–PCF, with half-metre length, using a direct chemical vapour deposition (CVD) growth method, which was previously considered to be extremely challenging due to the lack of a metal catalyst and the difficulties in gas flow control along the long micrometre-sized holes in silica PCF. Our success benefits from our extensive experience in the growth of graphene glass[35] and the good control of the molecular gas flow in confined space[36]. With this new Gr–PCF material, we have realized a greatly enhanced light–matter interaction between graphene and core-guided light, with ~8 dB cm^{-1} transmission attenuation. We have also demonstrated a tunable light–matter interaction by electrically gating graphene through an ionic liquid, with large modulation depth (~20 dB cm^{-1} at 1,550 nm) and broadband wavelength response (1,150–1,600 nm) under a low gate voltage (~2 V). The fully enhanced and tunable light–matter interaction in this Gr–PCF material indicates its great potential in all-fibre integration devices. Our results will pave a way for hybrid optical fibre manufacturing and suggest an exciting material platform of 2D material-integrated fibre with unprecedented function tunability in both linear and nonlinear optics.

[1]Centre for Nanochemistry, Beijing Science and Engineering Centre for Nanocarbons, Beijing National Laboratory for Molecular Sciences, College of Chemistry and Molecular Engineering, Peking University, Beijing, China. [2]Institute of Micro/Nano Photonic Materials and Applications, School of Physics and Electronics, Henan University, Kaifeng, China. [3]State Key Laboratory for Mesoscopic Physics, Academy for Advanced Interdisciplinary Studies, School of Physics, Peking University, Beijing, China. [4]Beijing Graphene Institute (BGI), Beijing, China. [5]Department of Electronics and Nanoengineering and QTF Centre of Excellence, Aalto University, Aalto, Finland. [6]Department of Physics, University of California at Berkeley, Berkeley, CA, USA. [7]These authors contributed equally: Ke Chen, Xu Zhou, Xu Cheng. *e-mail: khliu@pku.edu.cn; zfliu@pku.edu.cn

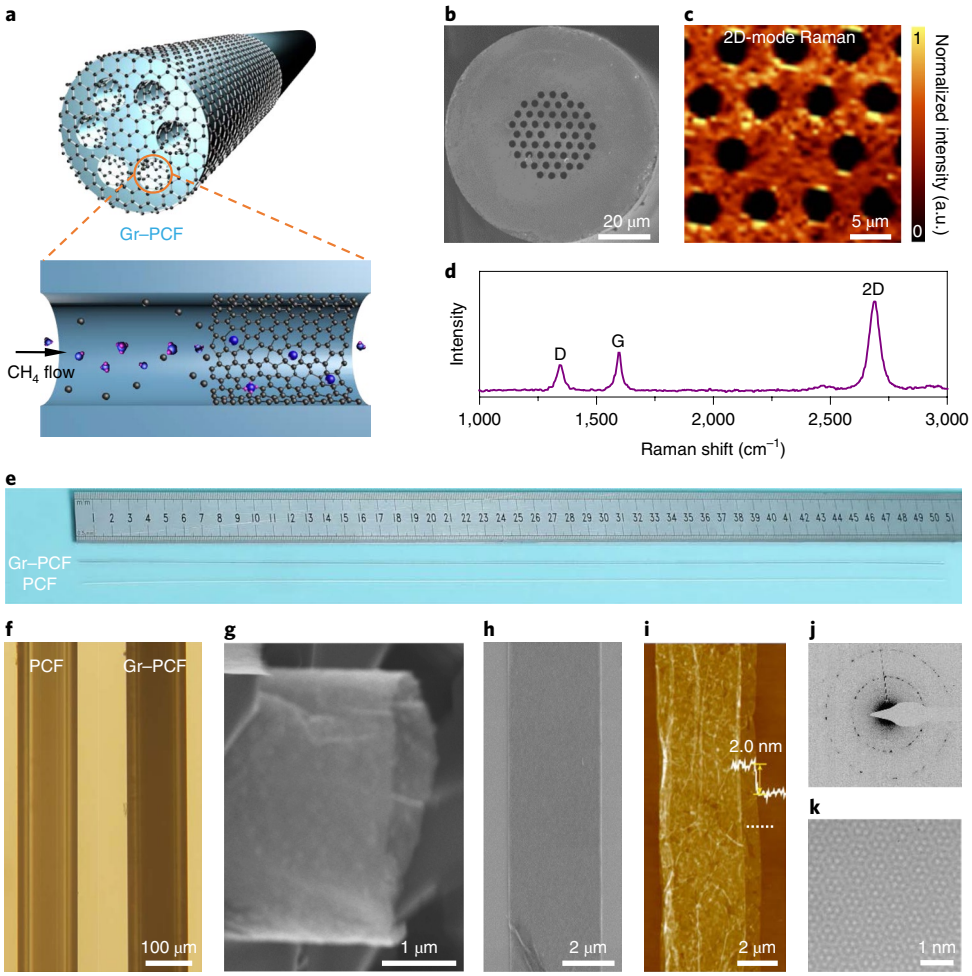

Fig. 1 | Growth and characterization of Gr–PCF. a, Schematics of Gr–PCF grown by the CVD method, with a graphene film on both the outer surface and inner walls of the PCF. **b**, Scanning electron microscopy (SEM) image of the Gr–PCF end surface. **c**,**d**, 2D-mode Raman intensity mapping (**c**) and Raman spectrum (**d**) of graphene at the fibre end surface. **e**,**f**, Optical reflection photograph (**e**) and transmission micrograph (**f**) of bare PCF and Gr–PCF. The optical contrast is darker for Gr–PCF due to light absorption by the graphene. **g**, SEM image of a tube-like graphene protruding out of one hole of the fractured Gr–PCF. **h**, SEM image of a graphene ribbon (the collapsed tube-like graphene grown on the hole wall) after dissolving the fibre silica. **i**, AFM image of a graphene ribbon with wrinkles. A height of ~2.0 nm is measured along the white dashed line. **j**,**k**, SAED (**j**) and HRTEM (**k**) images of the graphene ribbon.

In the present experiment, Gr–PCF was grown with methane (as the carbon feedstock) flowing through the narrow holes of the PCF (~4 μm in diameter), at ~1,100 °C and with controlled pressure (Fig. 1a). After growth, the PCF was able to maintain its structure, which consisted of a solid silica core and a surrounding cladding region with a patterned array of holes (Fig. 1b), while graphene was grown on both its outer surface and inner hole walls. The full covering of graphene on the outer surface was unambiguously confirmed by Raman mapping (Fig. 1c and Supplementary Fig. 1). The representative Raman spectrum in Fig. 1d shows sharp G- and 2D-mode peaks, revealing the high quality of the graphene (the observable D peak mainly comes from the defective grain boundaries between the graphene domains)[37]. The full covering of graphene on the inner hole walls is first indicated by the darker optical contrast of Gr–PCF than bare PCF due to light absorption by the graphene (Fig. 1e,f). Direct evidence of graphene growth inside the PCF is provided by the observation of tube-like graphene frameworks that tightly attach on the hole walls and protrude out of the holes when the Gr–PCF is broken (Fig. 1g and Supplementary Fig. 2). Furthermore, the inner graphene films can be directly obtained by dissolving the fibre silica in hydrofluoric acid (the graphene film on the outer surface was first removed by air-plasma treatment). The cylindroid graphene films from the Gr–PCF then collapse into ribbon films on the silicon substrate, with an average layer thickness of ~2.0 nm, as measured by atomic force microscopy (AFM, Fig. 1h,i). We note that the interlayer distance is relatively larger (estimated as 1.0–1.5 nm) than the intrinsic interlayer distance (0.34 nm) in these collapsed ribbons, probably due to the wrinkles formed during the etching treatment. The selected-area electron diffraction (SAED) image in Fig. 1j demonstrates the polycrystalline structure of the graphene film, as the selected-area aperture size (200 nm) is several times the graphene domain size (~50 nm). However, a high-resolution transmission electron microscopy (HRTEM) image of an individual graphene domain shows a perfect graphene lattice structure (the Moiré pattern of a bilayer is provided as an example in Fig. 1k). More TEM characterizations revealed that the graphene thickness can be controlled between one and ten layers by the growth time (Supplementary Fig. 3).

One great concern about the Gr–PCF growth is whether the graphene can be homogeneously distributed on the micrometre-sized hole walls along a long fibre, as gas flow in such a narrow space will have huge viscous force. To investigate this, we carried

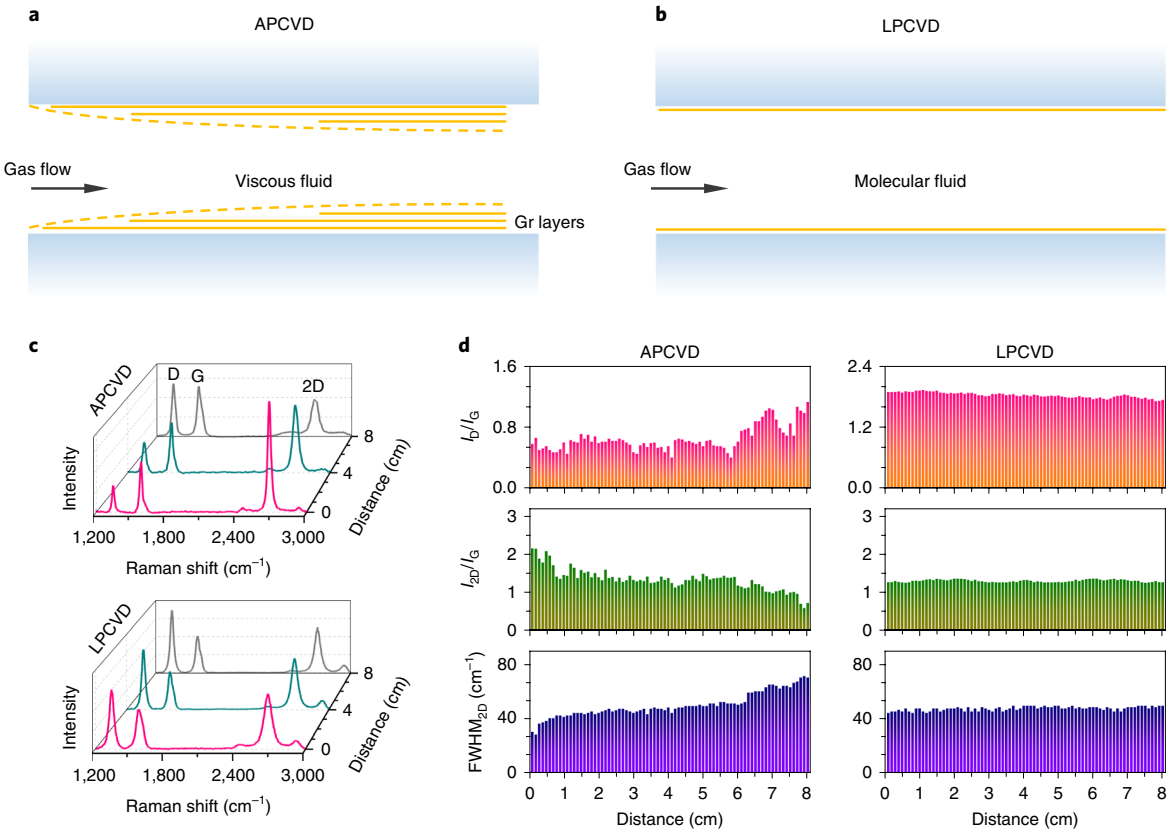

Fig. 2 | Controlled growth of a uniform graphene film on the hole walls of the PCF. a,**b**, Schematics of graphene growth on the walls of the micrometre-size holes of PCF with APCVD and LPCVD. **c**, Representative Raman spectra of graphene at different positions of the graphene ribbons along the gas flow under APCVD (top) and LPCVD (bottom) growth conditions. The graphene ribbons are taken from the hole walls after etching away the fibre silica. **d**, Statistics of the I_D/I_G, I_{2D}/I_G and $FWHM_{2D}$ of the graphene Raman peak at different positions of graphene ribbons by APCVD and LPCVD, where D, G and 2D are the D-, G- and 2D-mode Raman peaks of the graphene, respectively.

out control experiments with atmosphere-pressure CVD (APCVD, Fig. 2a) and low-pressure CVD (LPCVD, pressure of 0.5–1.0 kPa, Fig. 2b). According to the viscous flow model[38] (Supplementary Note 1), the mean free path of the carbon precursors (estimated as ~0.4 μm) is much shorter than the fibre hole diameter (~4 μm) under the atmosphere pressure of the APCVD process. In this situation, the carbon precursor feeding is limited by mass transfer[36]. According to experimental Raman data of graphene ribbons etched from the holes of Gr–PCF of ~8 cm length, the obvious variation of the 2D- to G-mode Raman (intensity ratio, I_{2D}/I_G, 0.6–2.1) and full-width at half-maximum 2D-mode ($FWHM_{2D}$, 31–71 cm^{-1}) results demonstrate the non-uniform thickness along the fibre axis (Fig. 2c,d, APCVD panels). This result is consistent with optical contrast observations, which show that the fibre becomes darker along the gas flow direction (Supplementary Fig. 4, lower fibre). This means that the graphene film thickness is increasing along the gas flow as a result of the increase in active carbon species during long-time thermal decomposition in downstream locations. In the LPCVD process, on the other hand, the gas flow approaches a free molecular flow situation, and the mass-diffusion process becomes negligible[36,38]. In this case, the mean free path (estimated as >40 μm) is much larger than the hole size of the PCF. The elapse time (~15 s) of gaseous molecules going through the long holes of the PCF in the LPCVD process is thus much shorter than that in the APCVD process (~175 s). It is facile to understand that the graphene films on the inner hole walls grow with uniform thickness along the fibre axis, as revealed by the Raman spectra, with negligible fluctuation of the I_{2D}/I_G ratio (~1.4) and $FWHM_{2D}$ (~48 cm^{-1}, Fig. 2c,d, LPCVD panels), as well as the uniform optical imaging contrast along the whole fibre (Supplementary Fig. 4, upper fibre). Here, we note that the D- to G-mode Raman intensity ratio (I_D/I_G) has a much larger value for LPCVD, indicating a smaller graphene domain size[37], originating from the reduced carbon feedstocks and corresponding to a slower growth rate and increased number of nucleation centres under molecular flow. Using a current furnace with a heating zone of ~60 cm, we can readily grow Gr–PCF with uniform thickness and length up to 50 cm (Fig. 1e).

In principle, one would expect that the light–graphene interaction in Gr–PCF would be greatly enhanced, as the atomic thickness of the graphene would not destroy the fundamental propagating mode. This assumption was checked by simulating the light electric field distribution of the fundamental guiding mode with the full-vector finite element method[30]. In the simulation, the graphene film directly interacts with the light field by evanescent wave coupling at the hole walls adjacent to the fibre core (Fig. 3a). Similar to the distribution in bare PCF (Supplementary Fig. 5d), the light in the Gr–PCF is mainly confined in the fibre core, and about one-tenth of the electric field compared to that at the fibre core centre is interacting with the graphene on the innermost hole walls (Fig. 3b). The light–graphene interaction is first indicated by the 3% kink in the normalized radial electric field distribution, which originates from the refractive index difference between the graphene/silica and air. The significantly enhanced light–graphene interaction in Gr–PCF can be quantitatively measured by the propagated light intensity evolution along the fibre. In bare PCF (~4 cm long) there is no observable attenuation (<0.01 dB cm^{-1}) at all (Fig. 3c,

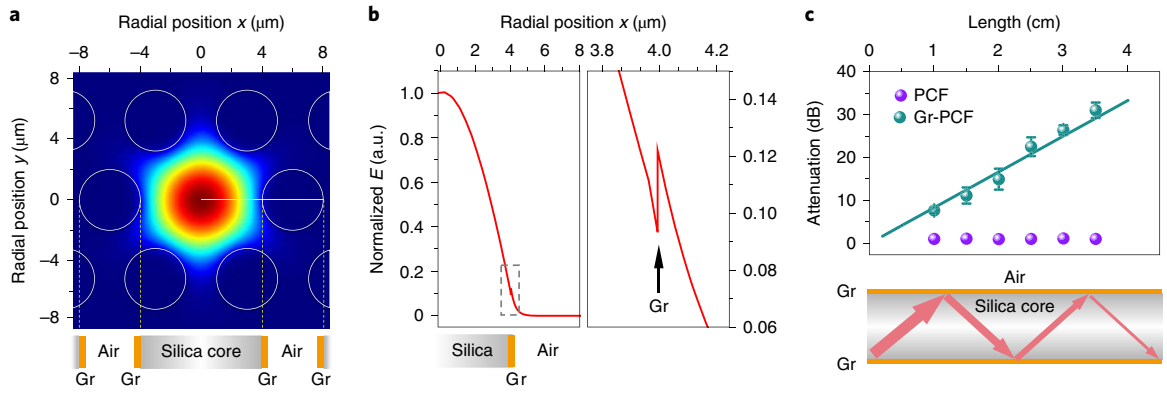

Fig. 3 | Strong light–matter interaction in Gr–PCF. a, Simulated light electric field distribution of the fundamental guiding mode at 1,550 nm. Graphene is set on the hole wall as shown in the profiles of the Gr–PCF (bottom, yellow rectangle). **b**, Distribution of the normalized electric field in the Gr–PCF along the horizontal radial direction (yellow horizontal line in **a**). Right, enlarged view of the dashed square in the left panel. The black arrow highlights the position of the graphene. **c**, Top, measured optical attenuation of light propagation in the bare PCF (purple dots) and Gr–PCF (cyan dots) with different fibre lengths. The attenuation coefficient is fitted as 8.3 dB cm^{-1} from the slope. Bottom, schematic of light attenuation with multiple reflections during its propagation along the Gr–PCF core. Error bars indicate s.d. from measurements of five samples for each length, grown under the same growth conditions.

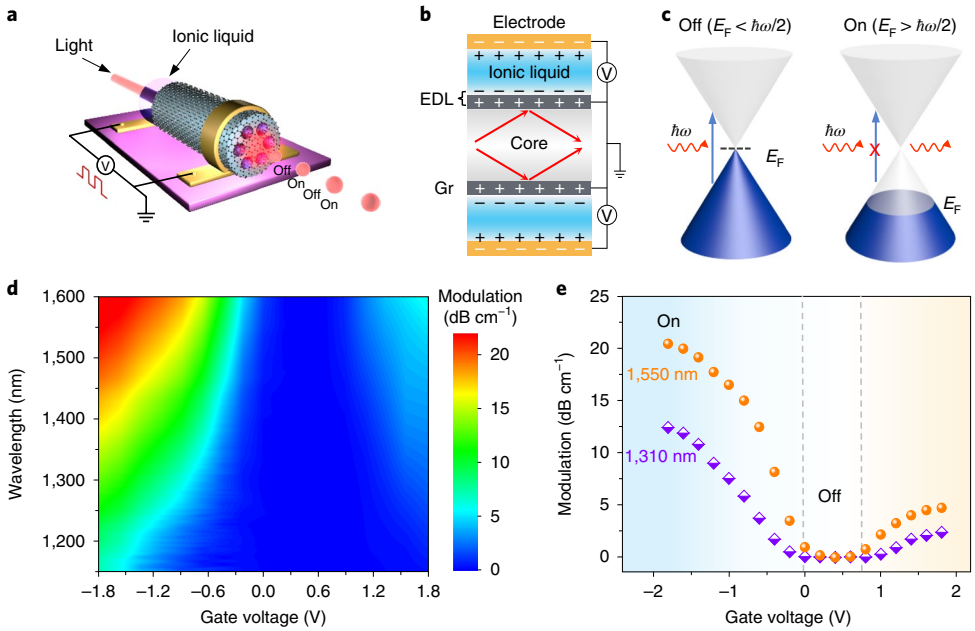

Fig. 4 | Tunable light–matter interaction in Gr–PCF. a, Schematic of a Gr–PCF-based electro-optic modulator. The gate voltage between the ionic liquid and graphene controls light transmission through the Gr–PCF. **b**,**c**, The working principle of the Gr–PCF electro-optic modulator, where an electrical double layer (EDL) forms at the interface between the graphene (dark grey rectangle) and ionic liquid (blue area). The ionic liquid-gating tunes the graphene's Fermi level and switches on and off the optical absorption in the graphene. When $E_F < \hbar\omega/2$ ($E_F > \hbar\omega/2$), graphene absorbs (does not absorb) light, and the modulator is working in the 'off' ('on') state for light transmission in the fibre. **d**, 2D mapping of transmission modulation (normalized by fibre length) of the Gr–PCF modulator as a function of gate voltage and optical wavelength. **e**, Modulation curves at 1,310 and 1,550 nm show an unambiguous transition between the 'on' and 'off' state with large modulation depth.

purple dots). However, in Gr–PCF, a strong attenuation of 8.3 dB cm^{-1} is observed (Fig. 3c, cyan dots, fitted slope), in striking contrast to the 0.1 dB in suspended monolayer graphene. The attenuation coefficient of this Gr–PCF is equivalent to an average graphene layer number of ~1.5 (Fig. 3c fit and Supplementary Fig. 5i). Here, the 0.5 layer comes from partial second graphene layers grown on the first graphene layer film. The greatly enhanced light–graphene interaction in Gr–PCF can be qualitatively understood by a tremendous enlargement of the effective interaction area and length during the multiple reflection of light propagation along the fibre axis (Fig. 3c, lower panel). Note that the light–graphene interaction strength can be tuned by the PCF geometry, for example via the air-hole diameter and hole pitch size (Supplementary Fig. 6).

One of the unique merits of 2D graphene is its unprecedented electrical tunability in the light–matter interaction by shifting its Fermi level (E_F)[21,26]. This tunability can be used to exploit the Gr–PCF as an in-line electro-optic modulator with intensity modulation in all-fibre communication networks (see testing set-up in Supplementary Fig. 7). Note that our Gr–PCF shows a stable and negligible loss (<0.1 dB) in

coupling with single-mode fibres. Here, we demonstrate an electro-optic modulator consisting of a short segment (0.5–1.5 cm) of Gr–PCF with ionic liquid (diethylmethyl(2-methoxyethyl)ammonium bis(trifluoromethylsulfonyl)imide, DEME-TFSI) inside the holes (Fig. 4a). The graphene on the hole walls of the Gr–PCF connects electrically with an electrode on the outside graphene surface (all the as-grown graphene films in the entire fibre are connected). Ionic liquid is then fully filled in the fibre holes and makes contact with another electrode. When a gate voltage is applied between the graphene and ionic liquid, an electrical double layer will form at the graphene–ionic liquid interface and dope graphene efficiently under a low gate voltage of several volts (Fig. 4b and Supplementary Fig. 8)[26,39,40]. Further simulation reveals an additional advantage of ionic liquid filling, in that it can increase the light–graphene interaction from 5 to 24 dB cm^{-1} for monolayer Gr–PCF by increasing the mode field area of the core-guided light (Supplementary Fig. 5), as ionic liquid has a refractive index (1.42) close to that of the PCF material (silica, 1.44).

By electrically tuning the graphene Fermi level via ionic liquid gating, the interband transition absorption can be tuned to the 'on' or 'off' state when E_F is smaller or larger than half a photon energy $\hbar\omega/2$, where ω and $\hbar\omega$ are the angular frequency and energy of a photon, respectively (Fig. 4c)[21,30]. This absorption-based electro-optic modulator operates at very low voltage (within 2 V) due to the efficient electrical double layer gating and the broadband spectral response from 1,150 to 1,600 nm due to the linear Dirac band structure of graphene (Fig. 4d). In particular, at the fibre-optic communication O- (1,310 nm) and C-wavelength bands (1,550 nm), the modulation depths can respectively reach ~13 and ~20 dB cm^{-1} at a gate voltage of −1.8 V (Fig. 4e). The relatively lower gating efficiency at the positive gate voltage region is attributed to the lower capacitance of our ionic liquid at the electron doping side, which is consistent with the electrical device measurements (Supplementary Fig. 8). The performance of our current modulator can be further improved. First, it has an insertion loss of ~6 dB cm^{-1} in the 'on' state, which can be much lower, in principle, if one grows very high-quality monolayer graphene on the inside walls of the PCF. Second, it has a slow switching speed of ~16 Hz (Supplementary Fig. 9), which can be improved (for example, a few tens of GHz[17,31]) if one can achieve optimized structures, such as Gr/hBN/Gr–PCF[41]. Nevertheless, the Gr–PCF modulator has high potential to be integrated with other optical devices in an all-fibre system where light can be simultaneously transmitted, modulated and detected inside the fibre link without the aid of discrete devices in the future[42].

In summary, we have demonstrated an ingenious CVD route to achieve a new material, Gr–PCF. The uniform and high-quality graphene on both the outer surface and inner hole walls of the PCF, with length up to half a metre, has been realized by low-pressure growth with controlled molecular flow. This Gr–PCF material exhibits a strong and tunable light–matter interaction and shows excellent performance as a broadband electro-optic modulator under a low gate voltage. With its electrical tunability, while maintaining its PCF waveguide mode intact and providing enhanced light–graphene interactions in both the linear and nonlinear optical regimes, Gr–PCF will soon enable novel fibre-optic devices such as electrically tunable mode-locked all-fibre lasers, gate-controllable wavelength-independent nonlinear wavelength converters, tunable broadband polarizers and optical limiters. In addition, our growth strategy will open up a new direction for the mass production of other 2D-crystal-based all-fibre devices, targeting next-generation optical fibres with various new functionalities.

Online content

Any methods, additional references, Nature Research reporting summaries, source data, statements of code and data availability and associated accession codes are available at https://doi.org/10.1038/s41566-019-0492-5.

Received: 12 December 2018; Accepted: 19 June 2019;
Published online: 12 August 2019

References

1. Russell, P. Photonic crystal fibers. *Science* **299**, 358–362 (2003).
2. Knight, J. C. Photonic crystal fibres. *Nature* **424**, 847–851 (2003).
3. Ouzounov, D. G. et al. Generation of megawatt optical solitons in hollow-core photonic band-gap fibers. *Science* **301**, 1702–1704 (2003).
4. Bartels, R. A. et al. Generation of spatially coherent light at extreme ultraviolet wavelengths. *Science* **297**, 376–378 (2002).
5. Couny, F., Benabid, F., Roberts, P. J., Light, P. S. & Raymer, M. G. Generation and photonic guidance of multi-octave optical-frequency combs. *Science* **318**, 1118–1121 (2007).
6. Dudley, J. M. & Taylor, J. R. Ten years of nonlinear optics in photonic crystal fibre. *Nat. Photon.* **3**, 85–90 (2009).
7. Jiang, X. et al. Deep-ultraviolet to mid-infrared supercontinuum generated in solid-core ZBLAN photonic crystal fibre. *Nat. Photon.* **9**, 133–139 (2015).
8. Benabid, F., Knight, J. C., Antonopoulos, G. & Russell, P. S. J. Stimulated Raman scattering in hydrogen-filled hollow-core photonic crystal fiber. *Science* **298**, 399–402 (2002).
9. Abouraddy, A. F. et al. Towards multimaterial multifunctional fibres that see, hear, sense and communicate. *Nat. Mater.* **6**, 336–347 (2007).
10. He, R. R. et al. Integration of gigahertz-bandwidth semiconductor devices inside microstructured optical fibres. *Nat. Photon.* **6**, 174–179 (2012).
11. Kottig, F. et al. Mid-infrared dispersive wave generation in gas-filled photonic crystal fibre by transient ionization-driven changes in dispersion. *Nat. Commun.* **8**, 813 (2017).
12. Rein, M. et al. Diode fibres for fabric-based optical communications. *Nature* **560**, 214–218 (2018).
13. Choi, S. Y. et al. Graphene-filled hollow optical fiber saturable absorber for efficient soliton fiber laser mode-locking. *Opt. Express* **20**, 5652–5657 (2012).
14. Martinez, A. & Sun, Z. P. Nanotube and graphene saturable absorbers for fibre lasers. *Nat. Photon.* **7**, 842–845 (2013).
15. Lin, Y.-H., Yang, C.-Y., Liou, J.-H., Yu, C.-P. & Lin, G.-R. Using graphene nano-particle embedded in photonic crystal fiber for evanescent wave mode-locking of fiber laser. *Opt. Express* **21**, 16763–16776 (2013).
16. Bao, Q. L. et al. Broadband graphene polarizer. *Nat. Photon.* **5**, 411–415 (2011).
17. Li, W. et al. Ultrafast all-optical graphene modulator. *Nano Lett.* **14**, 955–959 (2014).
18. Lee, E. J. et al. Active control of all-fibre graphene devices with electrical gating. *Nat. Commun.* **6**, 6851 (2015).
19. Zhang, Y. B., Tan, Y. W., Stormer, H. L. & Kim, P. Experimental observation of the quantum Hall effect and Berry's phase in graphene. *Nature* **438**, 201–204 (2005).
20. Novoselov, K. S. et al. Two-dimensional gas of massless Dirac fermions in graphene. *Nature* **438**, 197–200 (2005).
21. Wang, F. et al. Gate-variable optical transitions in graphene. *Science* **320**, 206–209 (2008).
22. Xia, F. N., Mueller, T., Lin, Y. M., Valdes-Garcia, A. & Avouris, P. Ultrafast graphene photodetector. *Nat. Nanotechnol.* **4**, 839–843 (2009).
23. Bonaccorso, F., Sun, Z., Hasan, T. & Ferrari, A. C. Graphene photonics and optoelectronics. *Nat. Photon.* **4**, 611–622 (2010).
24. Grigorenko, A. N., Polini, M. & Novoselov, K. S. Graphene plasmonics. *Nat. Photon.* **6**, 749–758 (2012).
25. Gan, X. T. et al. Chip-integrated ultrafast graphene photodetector with high responsivity. *Nat. Photon.* **7**, 883–887 (2013).
26. Polat, E. O. & Kocabas, C. Broadband optical modulators based on graphene supercapacitors. *Nano Lett.* **13**, 5851–5857 (2013).
27. Guo, Q. et al. Efficient electrical detection of mid-infrared graphene plasmons at room temperature. *Nat. Mater.* **17**, 986–992 (2018).
28. Romagnoli, M. et al. Graphene-based integrated photonics for next-generation datacom and telecom. *Nat. Rev. Mater.* **3**, 392–414 (2018).
29. Nair, R. R. et al. Fine structure constant defines visual transparency of graphene. *Science* **320**, 1308–1308 (2008).
30. Liu, M. et al. A graphene-based broadband optical modulator. *Nature* **474**, 64–67 (2011).
31. Phare, C. T., Lee, Y. H. D., Cardenas, J. & Lipson, M. Graphene electro-optic modulator with 30 GHz bandwidth. *Nat. Photon.* **9**, 511–514 (2015).
32. Lin, H. T. et al. Chalcogenide glass-on-graphene photonics. *Nat. Photon.* **11**, 798–805 (2017).
33. Sorianello, V. et al. Graphene–silicon phase modulators with gigahertz bandwidth. *Nat. Photon.* **12**, 40–44 (2018).
34. Yao, B. C. et al. Gate-tunable frequency combs in graphene–nitride microresonators. *Nature* **558**, 410–414 (2018).
35. Sun, J. Y. et al. Graphene glass from direct CVD routes: production and applications. *Adv. Mater.* **28**, 10333–10339 (2016).

36. Wang, H. et al. Surface monocrystallization of copper foil for fast growth of large single-crystal graphene under free molecular flow. *Adv. Mater.* **28**, 8968–8974 (2016).
37. Sato, K. et al. D-band raman intensity of graphitic materials as a function of laser energy and crystallite size. *Chem. Phys. Lett.* **427**, 117–121 (2006).
38. Knudsen, M. *The Kinetic Theory of Gases* (Methuen, 1952).
39. Ye, J. T. et al. Liquid-gated interface superconductivity on an atomically flat film. *Nat. Mater.* **9**, 125–128 (2010).
40. Fujimoto, T. & Awaga, K. Electric-double-layer field-effect transistors with ionic liquids. *Phys. Chem. Chem. Phys.* **15**, 8983–9006 (2013).
41. Yang, W. et al. Epitaxial growth of single-domain graphene on hexagonal boron nitride. *Nat. Mater.* **12**, 792–797 (2013).
42. Yamashita, S. Nonlinear optics in carbon nanotube, graphene and related 2D materials. *APL Photon.* **4**, 034301 (2019).

Acknowledgements

This work was supported by the National Key R&D Program of China (2016YFA0200103, 2016YFA0300903, 2016YFA0300804), Beijing Graphene Innovation Program (Z181100004818003, Z161100002116028), NSFC (51432002, 51520105003, 51502077, 51522201, 11474006), Beijing Municipal Science & Technology Commission (Z181100004218006), the National Equipment Program of China (ZDYZ2015-1), the Postdoctoral Innovative Personnel Support Program (BX20180013), The Science and Technology Development Project of Henan Province (182102210029), Zhongyuan Thousand Talents Program of Henan Province, the Young Talents Program of Henan University, the Director, Office of Science, Office of Basic Energy Sciences, Materials Sciences and Engineering Division of the US Department of Energy under contract no. DE-AC02-05-CH11231 (SP2 program), the Academy of Finland (276376, 295777, 312297, 314810), the Academy of Finland Flagship Programme (320167, PREIN), the ERC (834742) and the European Union's Horizon 2020 research and innovation programme (820423, S2QUIP)

Author contributions

Z.L. and K.L. supervised the project. Z.L. and K.C. conceived the material growth. K.L. and X.Z. conceived the optical measurement. K.C. and X.Z. carried out the material growth experiment and optical device measurements. X.C. performed theoretical modelling. K.C., R.Q., Y.C., Y.X., X.Z., C.L. and F.Y. conducted SEM, TEM, AFM and Raman characterizations. W.Y. suggested the optical experiments. F.Y. programmed the measurement software. Z.S. and F.W. suggested the modulator. All authors contributed to the scientific discussion and writing of the manuscript.

Competing interests

The authors declare no competing interests.

Additional information

Supplementary information is available for this paper at https://doi.org/10.1038/s41566-019-0492-5.

Reprints and permissions information is available at www.nature.com/reprints.

Correspondence and requests for materials should be addressed to K.L. or Z.L.

Publisher's note: Springer Nature remains neutral with regard to jurisdictional claims in published maps and institutional affiliations.

Methods

Growth of Gr–PCFs. The PCFs (125 μm cladding diameter and 8 μm core diameter) were placed in the centre of a tube furnace (Thermo Linderberg). For the APCVD process, methane (10 s.c.c.m.) was introduced as a carbon feedstock with Ar (100 s.c.c.m.) and H_2 (50 s.c.c.m.) at 1,100 °C for hours under atmosphere pressure. For the LPCVD process, methane (50 s.c.c.m.) was mixed with H_2 (50 s.c.c.m.) at 1,100 °C for hours under a pressure of 500–1,000 Pa. After growth, the as-grown sample was naturally cooled in the protective gases Ar and H_2.

Characterization of Gr–PCFs. An optical microscope (Olympus BX51) was used to obtain optical images. SEM images were collected using an FEI Nova Nano-SEM430 device at 5 kV. Raman spectra and mappings were obtained with a WITec alpha 300R-confocal Raman imaging system equipped with a 532 nm laser. AFM pictures and data were taken in a Bruker Dimension Icon atomic force microscope. HRTEM and SAED experiments were performed in an aberration-corrected FEI Titan Themis G2-300 system at 80 kV.

Numerical modelling. Numerical simulations were processed using the RF module of COMSOL Multiphysics software and MATLAB software. The effective refractive index of the fundamental guiding mode in Gr–PCFs was calculated using the finite element method in COMSOL.

Device fabrication and modulation measurements. Ti/Au (5/100 nm) electrodes were deposited on the graphene film by electron-beam evaporation. The ionic liquid (DEME-TFSI, Sigma-Aldrich) was injected into the holes in the Gr–PCF with another Ti/Au electrode connection. The two ends of the Gr–PCF were connected with two single-mode optical fibres (SMFs, Corning SMF-28e+) and the gap between the fibres was filled with ionic liquid. The two SMFs were aligned with the Gr–PCF using our home-built set-up (Supplementary Fig. 6), allowing two optical microscopic observations in different directions and using multi-axis piezo-stages to ensure accurate alignment. A Keithley 2400 Source Meter provided the gate voltage. A supercontinuum laser (NKT Photonics) was coupled into the SMF to provide broadband light. The modulated signal was sent into a spectrograph equipped with an infrared CCD (Princeton Instruments, Acton SpectraPro SP-2300 and Pylon-IR 1024–1.7).

Data availability

The data that support the plots within this paper and other findings of this study are available from the corresponding author upon reasonable request.